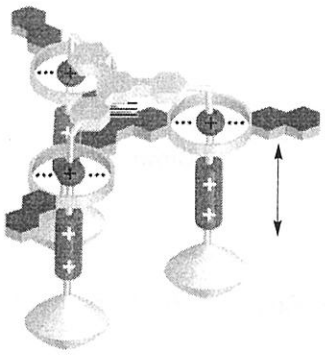

elevator

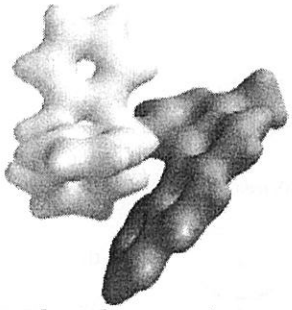

molecular ratchet

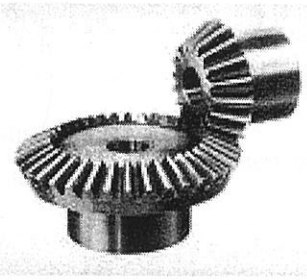

bevel gear

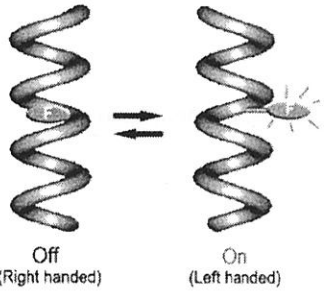

Molecular Switch

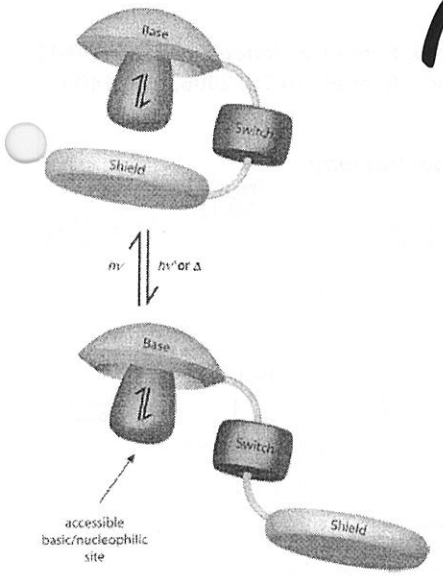

photo switching of basicity

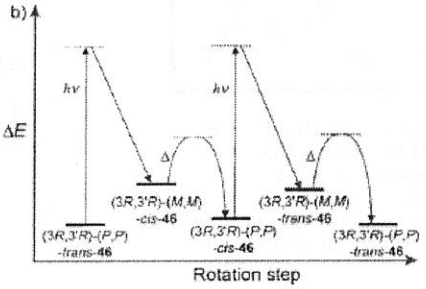

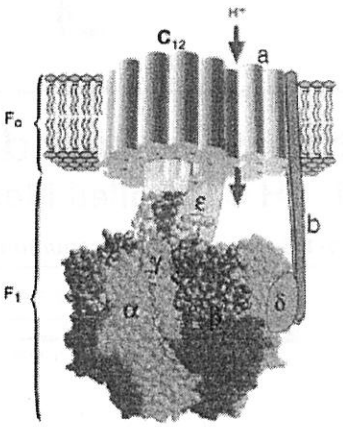

naturally occurring rotary motor F1-ATPase

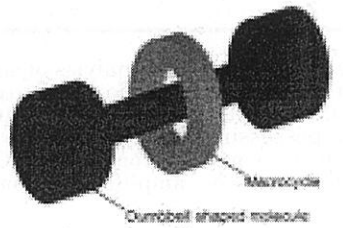

image of rotaxane

ref. ***ACIE***, **2007**, *46*, 72

<< Contents >>

Hetch, S. et al, ***ACIE***, **2008**, *47*, 5968

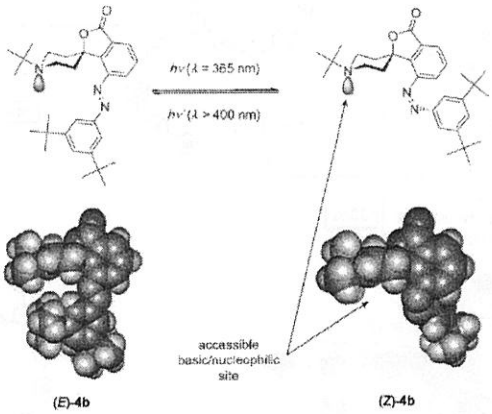

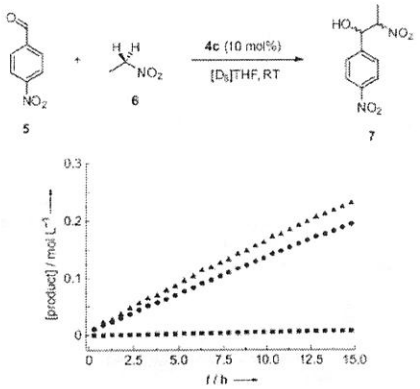

Figure 3. Perfomance of the photoswitchable piperidine 4c in its two switching states as general base catalyst for the Henry reaction of 5 with 6 to give 7: ■ (*E*)-4c, ● (*Z*)-4c in the photostationary state with residual (*E*)-4c, ▲ extrapolation to 100% (*Z*)-4c with a correction for the thermal (*Z*)-4c→(*E*)-4c back reaction. Reaction conditions: catalyst (10 mol%), 4-nitrobenzaldehyde (0.40 M, 1 equiv), nitroethane (12 equiv), [D8]THF, 25 °C.

1. Introduction

Catenane

Wasserman, E. ***JACS***, **1960**, *82*, 4433

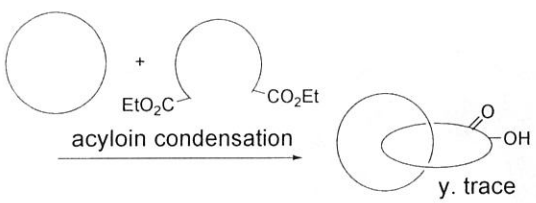

Rotaxane

Harrison, S. et al, ***JACS***, **1967**, *89*, 5723

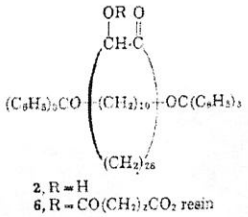

Crown Ether

Pederson, C. J. et al, ***JACS***, **1967**, *89*, 7017

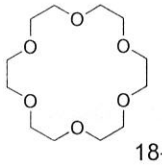

18-Crown-6

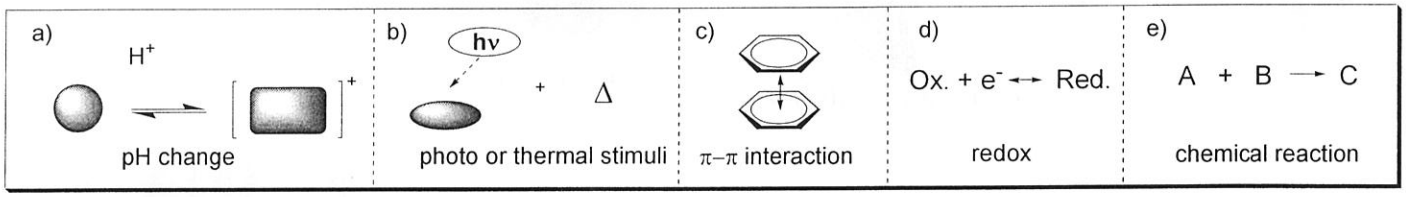

2. Rotaxane Based Molecular Switch

2-1. pH Controlled Molecular Elevator

Credi, A.; Stoddart, J. F. et al. ***Science,*** **2004,** *303*, 1845
Stoddart, J. F.; Credi, A. et al. ***JACS,*** **2006,** *128*, 1489

Fig. 2-1-1 Schematic Representation of Switchable Rotaxane

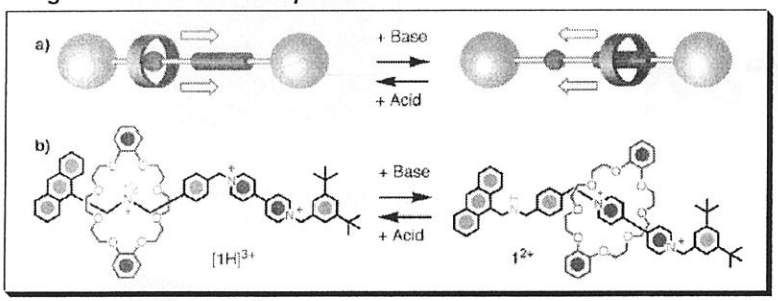

X-Ray crystallographic analysis of single crystals obtained from a solution containing equimolar quantities of DB24C8 and DBA·PF_6 revealed the formation in the solid state of the expected 1:1 complex, possessing a pseudorotaxane geometry.
It means they prefer strong [$^+$N–H···O] hydrogenbonding and weak [C–H···O] interaction, amplified by some stablizing [π·π] stacking forces.

Fig. 2-1-2 HRMS Spectrometry

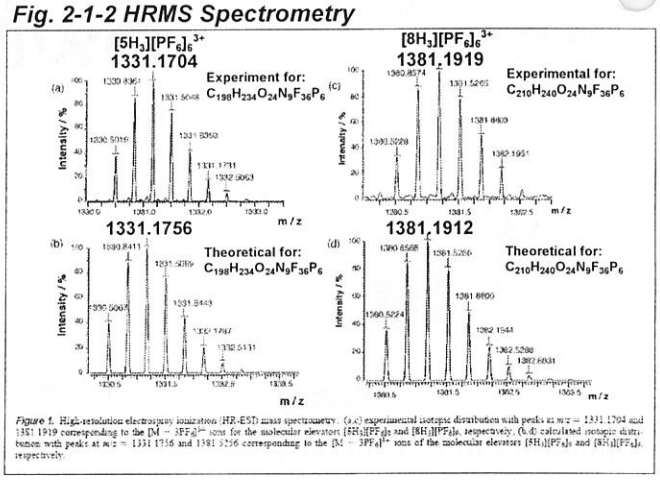

Figure 1. High-resolution electrospray ionization (HR-ESI) mass spectrometry. (a,c) experimental isotopic distribution with peaks at m/z = 1331.1704 and 1381.1919 corresponding to the $[M - 3PF_6]^{3+}$ ions for the molecular elevators $[5H_3][PF_6]_9$ and $[8H_3][PF_6]_9$, respectively. (b,d) calculated isotopic distribution with peaks at m/z = 1331.1756 and 1381.1912 corresponding to the $[M - 3PF_6]^{3+}$ ions of the molecular elevators $[5H_3][PF_6]_9$ and $[8H_3][PF_6]_9$, respectively.

Schemne 2-1-1 Synthesis of Molecular Elevators

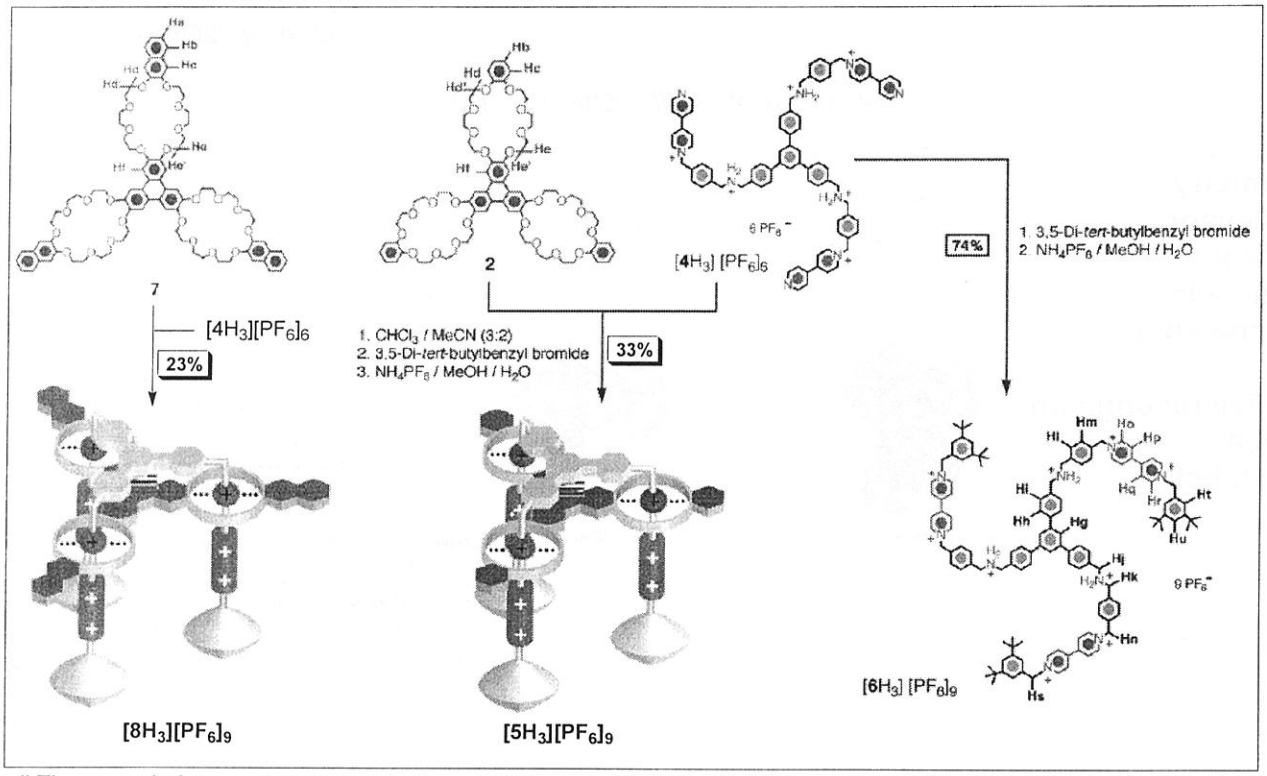

The extended aromatic units confer stronger electrondonating power compared with the simple benzo units? ([5H_3][PF_6]$_9$ vs. [8H_3][PF_6]$_9$)

Fig. 2-1-3 ^{1}H NMR Study

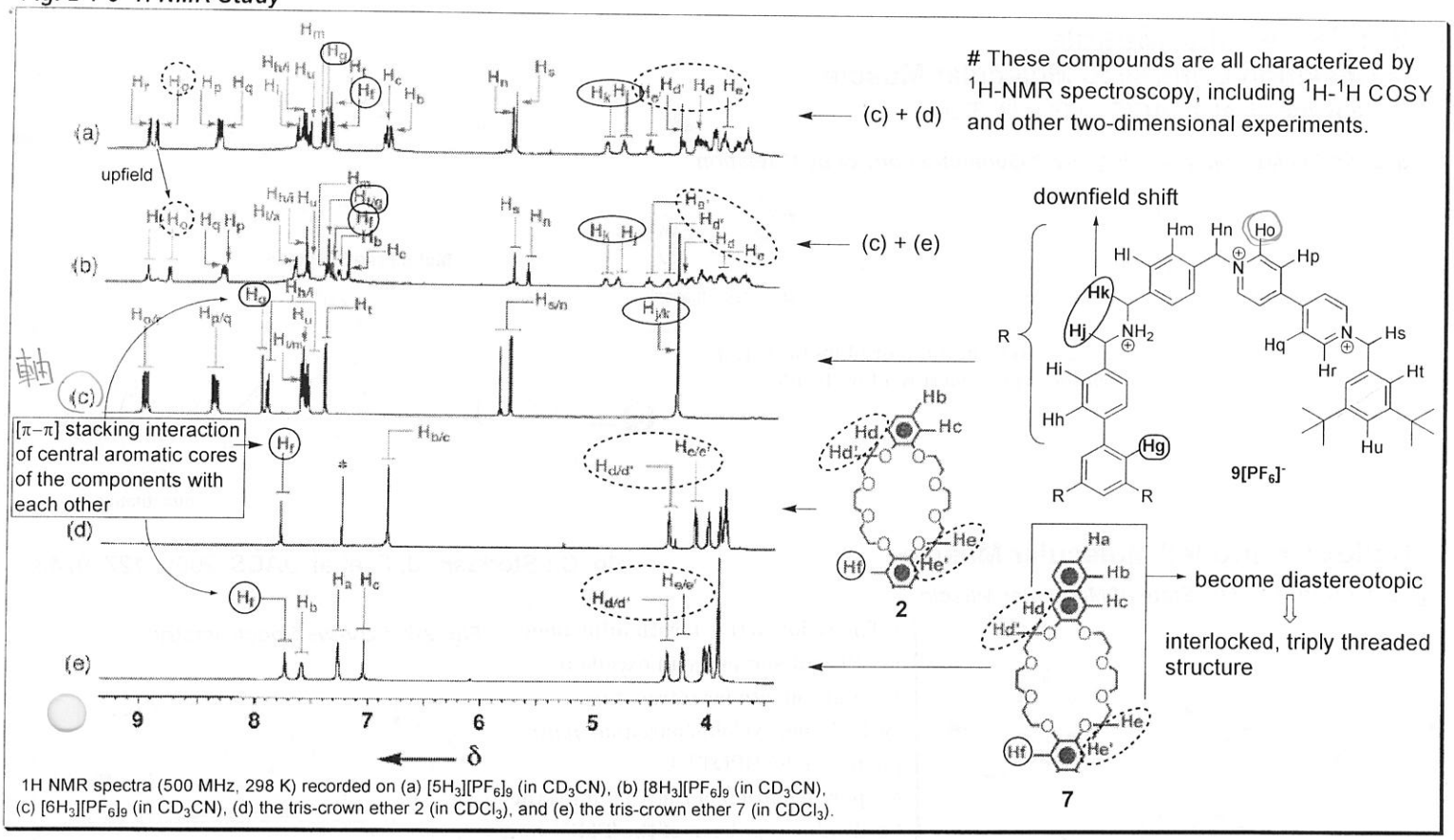

1H NMR spectra (500 MHz, 298 K) recorded on (a) $[5H_3][PF_6]_9$ (in CD_3CN), (b) $[8H_3][PF_6]_9$ (in CD_3CN), (c) $[6H_3][PF_6]_9$ (in CD_3CN), (d) the tris-crown ether 2 (in $CDCl_3$), and (e) the tris-crown ether 7 (in $CDCl_3$).

These compounds are all characterized by ^{1}H-NMR spectroscopy, including ^{1}H-^{1}H COSY and other two-dimensional experiments.

Table 2-1-1 Switching Process Using Different Bases

base	pK_a MeCN	solvent	temperature/ K	deprotonation
1,8-diazabicyclo[5.4.0]-undec-7-ene (DBU)	18.3	CD_3CN	298	decomposition of $BIPY^{2+}$ units
1,4-diazabicyclo[2.2.2]-octane (DABCO)	18.3	CD_3CN	298	incomplete, reversible[a,b]
potassium hexamethyldisilazane (KHMDSZ)	26.0[a]	CD_3CN	298	decomposition of $BIPY^{2+}$ units
quinuclinide	9.80[a]	CD_3CN	298	incomplete, reversible[b]
2,6-lutidine	14.0	CD_3CN	298	incomplete, reversible[b]
potassium *tert*-butoxide (*t*-BuOK)	19.0[a]	CD_3CN	298	decomposition of $BIPY^{2+}$ units
N-ethyldiisopropylamine (EDIPA)	11.4[a]	$(CD_3)_2CO$, CD_3CN, $(CD_3)_2SO$	235–298	incomplete, reversible[b]
tributylamine (TBA)	18.0	CD_3CN	298	incomplete, reversible[b]
N,N,N',N'-tetramethyl-1,8-naphthalene-diamine (proton-sponge)	18.2	$(CD_3)_2CO$	298	incomplete, reversible[b]
N-*tert*-butyl-*N',N',N'',N''',N''',N'''*-hexamethyl-phosphorimidic triamide (P_1-*t*-Bu)	26.5	CD_3CN	298	complete, reversible[b]

[a] In DMSO [b] Upon addition of TFA

A mechanically interlocked molecular bundle can be fully deprotonated when it is subjected to very strong base.

P_1-*t*-Bu =

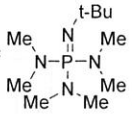

Fig. 2-1-4 ^{1}H NMR Study

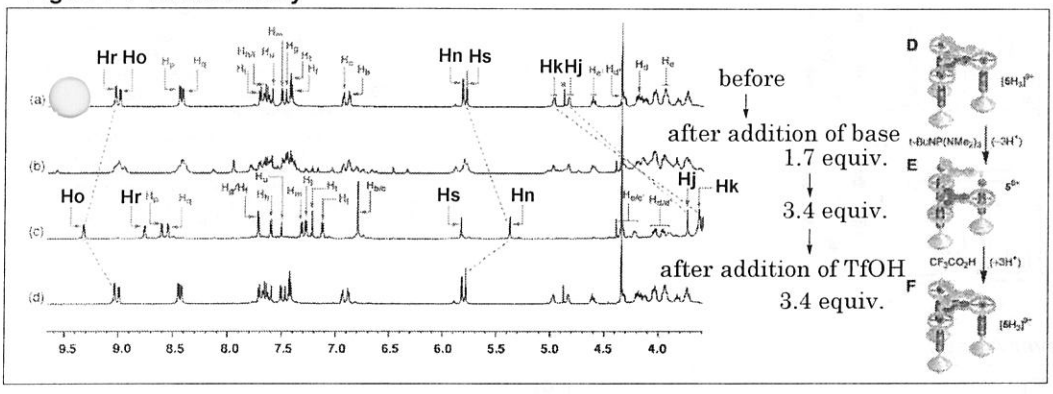

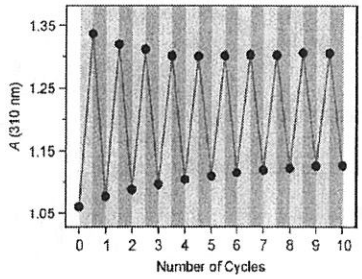

Changes in absorbance observed at 310 nm (path length is 4.0 cm) for a 7.1 μM solution of $[5H_3]^{9+}$ on successive addition of stoichiometric amounts of base (yellow areas) and acid (green areas). All experiments were carried out in acetonitrile solution at 298 K.

Scheme 2-1-2 Base-Acid Controlled Mechanical Switching

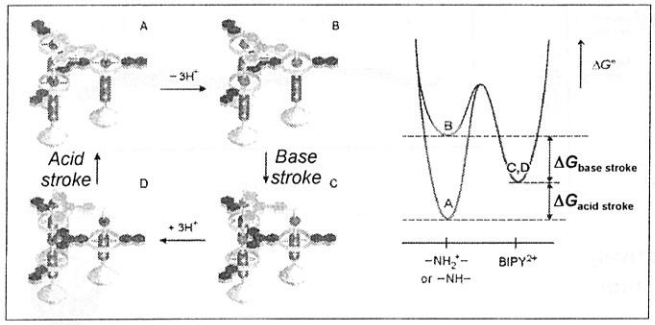

The negative shift of the potential for the reductions of the $BIPY^{2+}$ units with respect to the rig component is larger for 8^{6+} than it is for 5^{6+}. Such a larger shift, which indicates that the $BIPY^{2+}$ units experience stronger electron donor-acceptor interactions in the former elevator(dioxynaphthalene) than in the latter(dioxybenzene).

Because molecular models show that the distance traveled by the platform is about 0.7 nm, they speculate that the elevators could potentially generate a maximum force of around 200 pN in the base stroke. Such force is more than 1 order of magnitude larger than the forces developed by natural linear motors like myosin and kinesin.

2-2. Molecular Muscle

> Chelation Controlled Molecular Muscle

Sauvage, J. et al. *ACIE*, 2000, *39*, 3284

Fig. 2-2-1 Skeletal Muscle

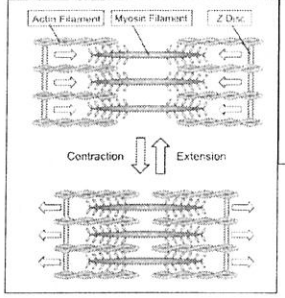

Fig. 2-2-2 Geometry control by Chelation

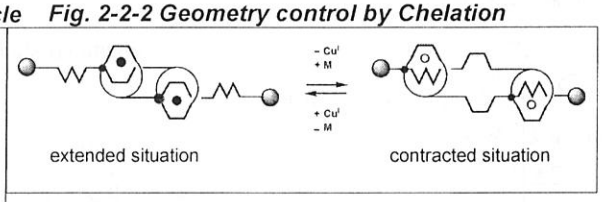

The coordination number of metal cation determines the structure of molecules.

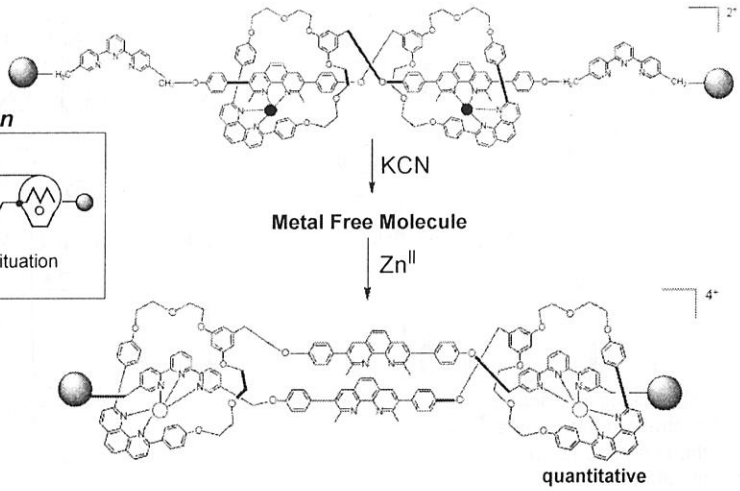

> Redox Controlled Molecular Muscle

Ho, C.; Stoddart, J. F. et al. *JACS*, 2005, *127*, 9745

Fig. 2-2-2 Red. and Ox. State of Molecular Muscle

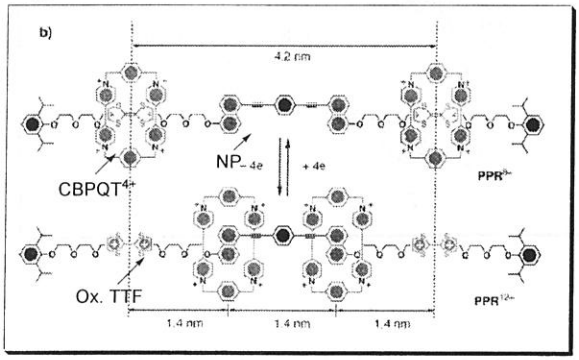

The redox-active terathiafluvalene (TTF) unit serves as an excellent recognition site for tetracationic cyclophane, cyclobis(paraquat-*para*-phenylene)(CBPQT^{4+}).

Upon oxidation of the TTF unit, the Coulombic repulsion of the TTF^{2+} unit provides a powerful "push-pull" mechanism for the translocation of the CBPQT^{4+} ring.

Fig. 2-2-3 ^{1}H-NMR in Acetone-d^{6}

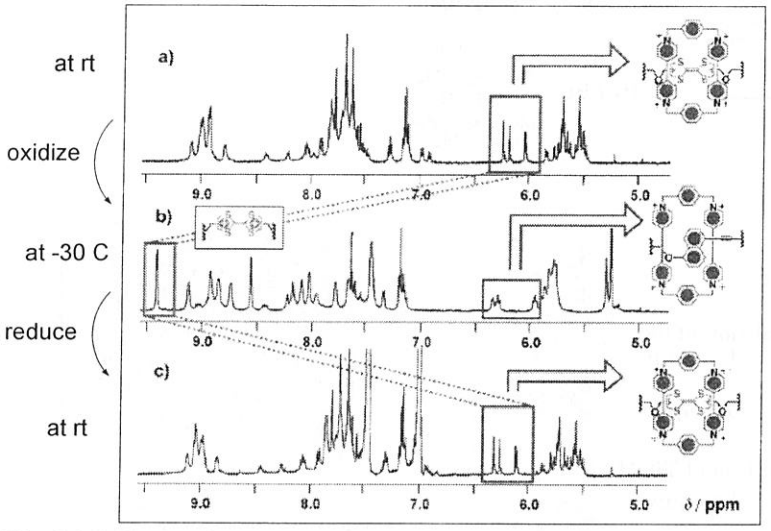

Fig. 2-2-4 UV-vis Spectrometry

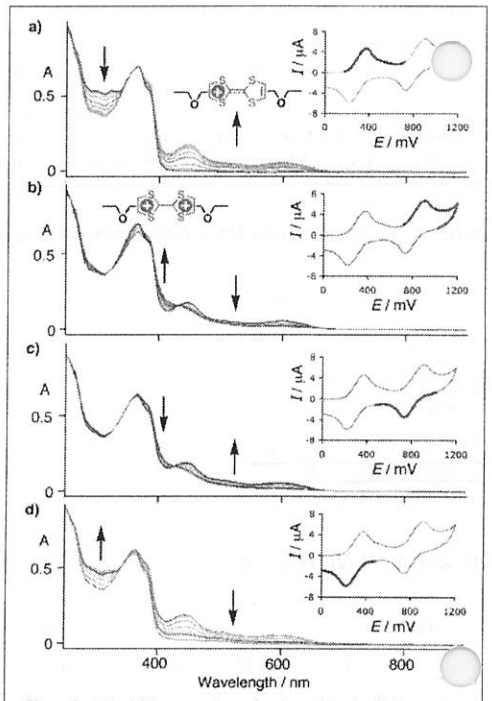

Figure 9. UV—visible spectroelectrochemistry of the dumbbell **PPD** (~1 × 10^{-3} mol L^{-1}, CH_2Cl_2, 0.1 mol L^{-1} $TBAPF_6$) recorded simultaneously with a CV (inset, 0.2 mV s^{-1}) showing the corresponding growth and bleach of the related chromophores. The voltage ranges that account for the spectroscopic changes are marked on the CV in bold and correspond to the formation of TTF-based (a) monocations **PPD**$^{3+/2+}$ and (b) dications **PPD**$^{4+}$ together with the reverse reformation of (c) the monocations and (d) neutral forms.

Fig. 2-2-5 Mechanical Actuation of Cantilever Arrays

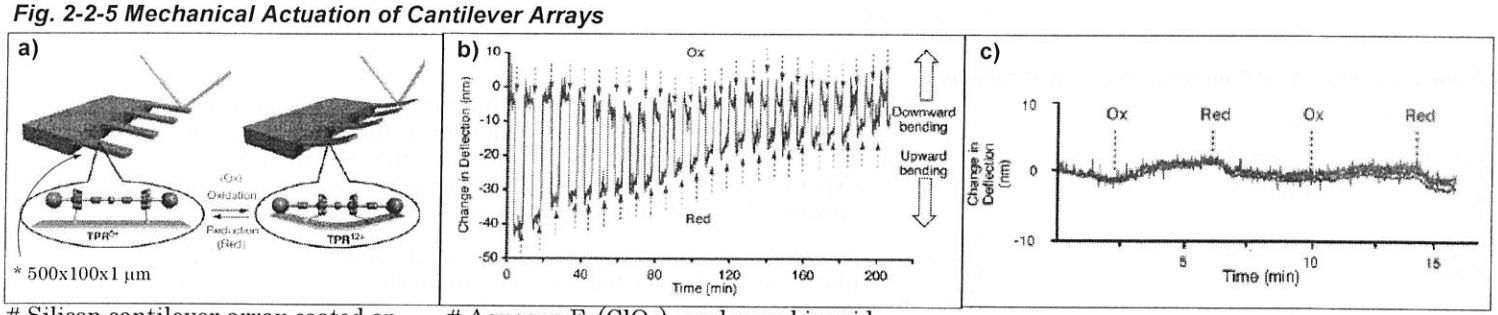

Silicon cantilever array coated on its topside with a 20 nm thin layer of gold was coated with the muscle molecules.

Aqueous $Fe(ClO_4)_3$ and ascorbic acid solutions were sequentially and alternatively introduced into the fluid cell under constant flow (250-300 μL/min).

3. Rotary Molecular Motor

3-1. Enantioselective Recognition

> Metal Bisporphyrine Double Deckers

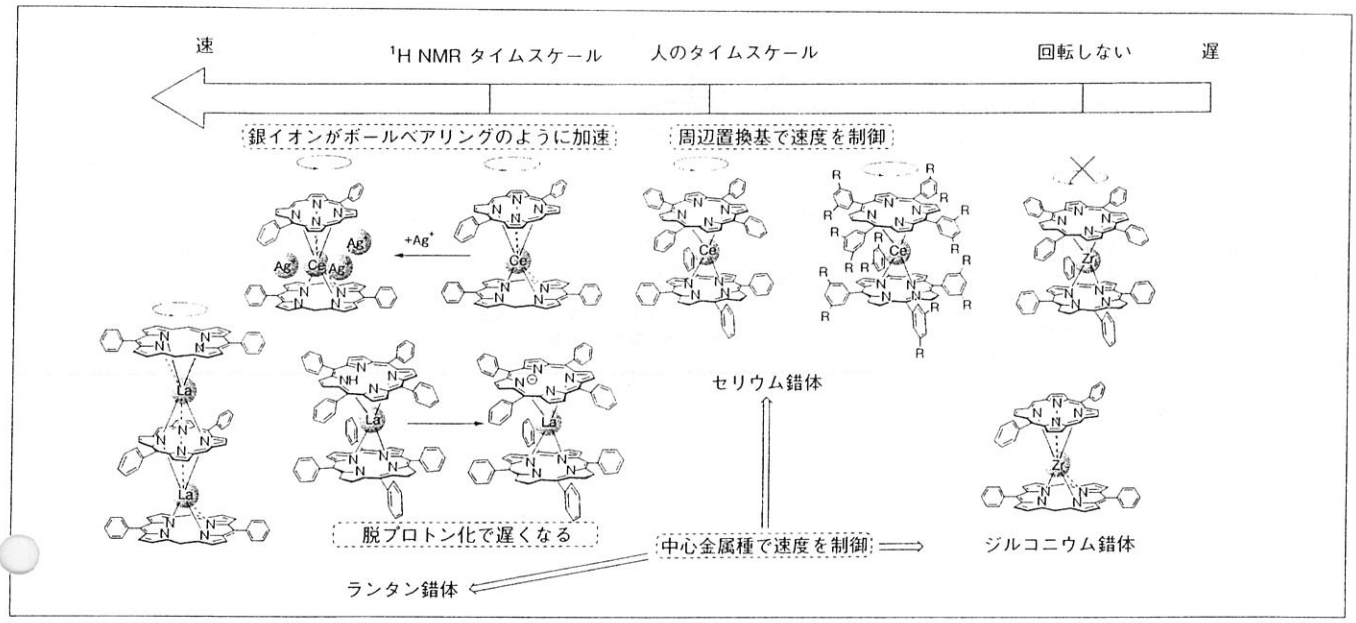

> Allosteric Systems for Amplification of Guest Affinity and Selectivity

Shinkai, S. et al. *Acc. Chem. Res.* **2001**, *34*, 494

Fig. 3-1-2 Negative Allosteric Systems

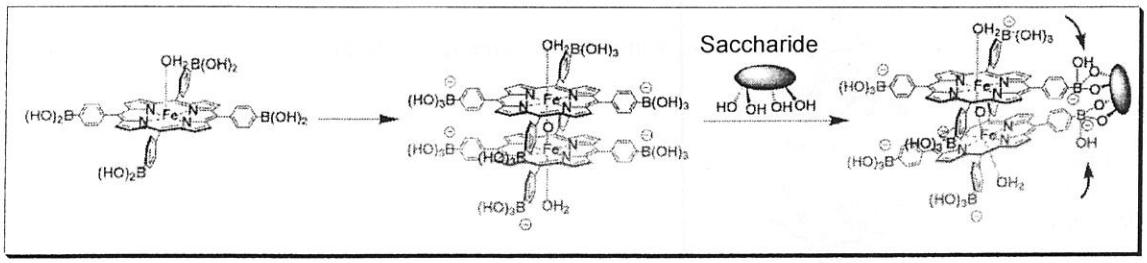

When two boronic acids react with four saccharide OH groups, they must get close to each other and the Fe-O-Fe bond angle is tilted to 150. Then the distance between two boronic acids becomes too long to complex saccharides intramolecularly. So, this binding mode is classified as negative homotropic allosterism.

Fig. 3-1-3 Positive Allosteric Systems

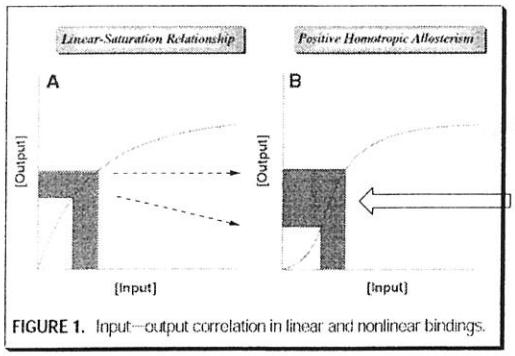

FIGURE 1. Input–output correlation in linear and nonlinear bindings.

15a has a sharp positive allosteric effect.
The binding of these chiral guests can be monitored by observing CD spectral.

Scheme 3-1-1

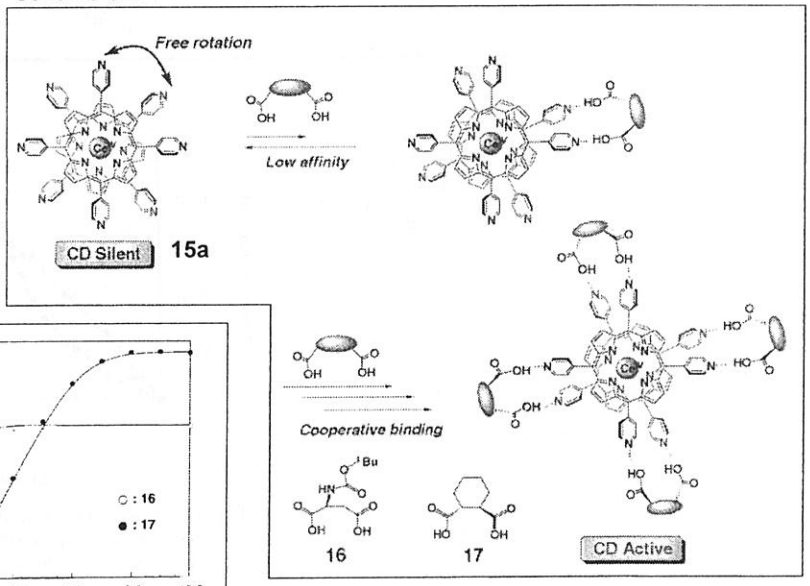

Fig. 3-1-3

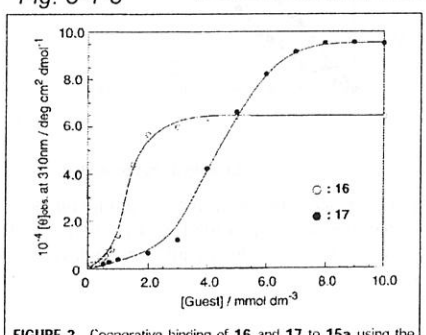

FIGURE 2. Cooperative binding of **16** and **17** to **15a** using the hydrogen-bonding interaction.[37]

> Highly Enantioselective Recognition

Takeuchi, M.; Shinkai, S. et al. *JACS*, **2006**, *128*, 16008

Fig. 3-1-4 Schematic Illustration of DDPy7-R

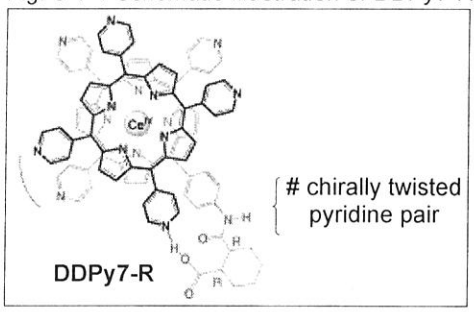

DDPy7-R exhibits extremely hight enantioselectivity toward RR-CHDA even under the conditions of -20% ee.

The information of an error molecule is filtered off by the control of nonlinear responses.

Fig. 3-1-5 CD Spectroscopic Titrations at 310 nm

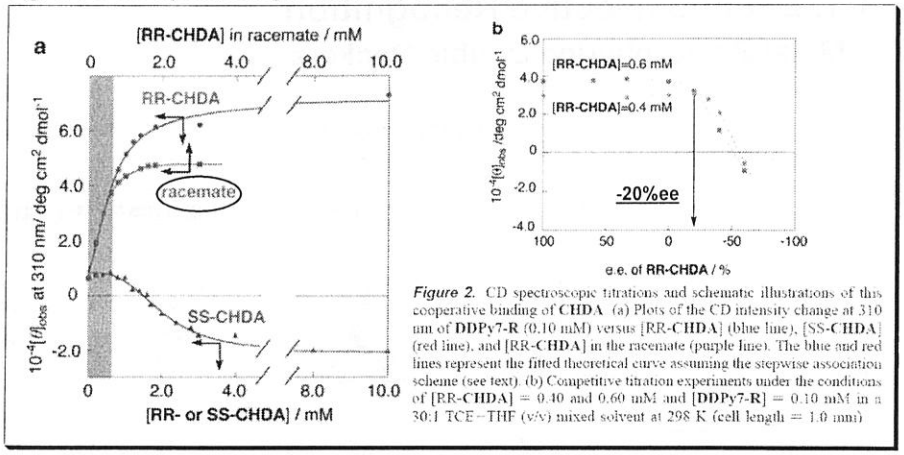

Figure 2. CD spectroscopic titrations and schematic illustrations of this cooperative binding of **CHDA**. (a) Plots of the CD intensity change at 310 nm of **DDPy7-R** (0.10 mM) versus [RR-**CHDA**] (blue line), [SS-**CHDA**] (red line), and [RR-**CHDA**] in the racemate (purple line). The blue and red lines represent the fitted theoretical curve assuming the stepwise association scheme (see text). (b) Competitive titration experiments under the conditions of [RR-**CHDA**] = 0.40 and 0.60 mM and [**DDPy7-R**] = 0.10 mM in a 30:1 TCE–THF (v/v) mixed solvent at 298 K (cell length = 1.0 mm).

> Allosteric Potassium(I) Ion Binding

Shinkai, S. et al. *Bull. Chem. Soc. Jpn.*, **2001**, *74*, 883

Scheme 3-1-2 Synthesis of Crown Ether Double Decker

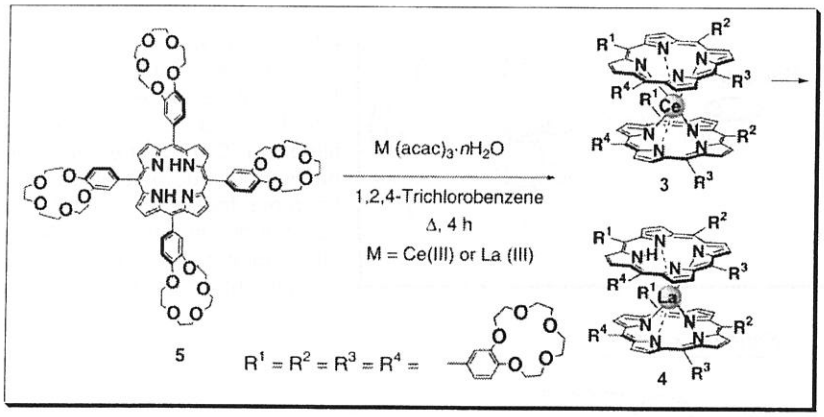

impossible to purify satisfactory

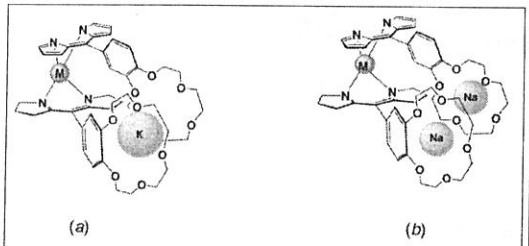

Fig. 3. Schematic representation of the difference between the binding mode of K^+ (*a*) and Na^+ (*b*). In the case of K^+, a single ion spans two crown ethers from separate porphyrin moieties which aligns the remaining crown ethers and leads to nonlinear complexation. The smaller Na^+ ions, however, can fit within individual crown cavities independently of each other. This behavior leads to linear complexation.

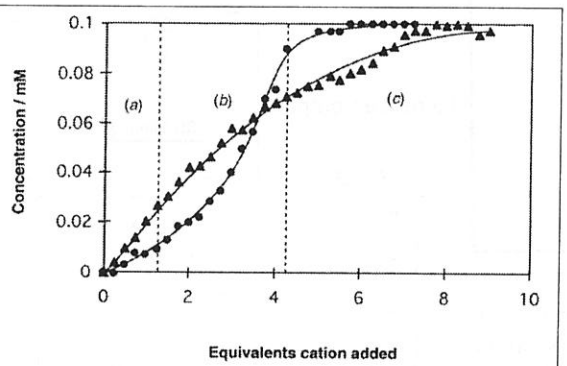

Fig. 4. Concentration profile of cation complexed double decker porphyrin upon titrating **4** (1:1 $CHCl_3$/MeCN, 1.0×10^{-4} mol dm^{-3}) with $NaPF_6$ (triangles) or KPF_6 (circles).

3-2. Molecular Gear

> Thiazolyl Disk-Shaped Ligand

Shionoya, M. et al. *JACS*, **2004**, *126*, 1214
Hiraoka, S.; Shionoya, M. et al. *JACS*, **2008**, *130*, 9089

Fig. 3-2-1 Heterotopic Sandwich-Shaped Complex

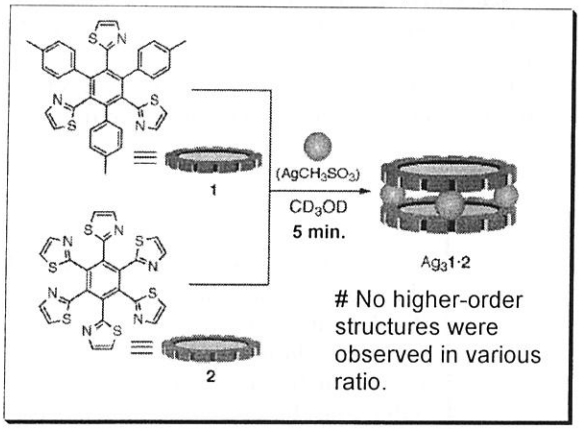

*Scheme 3-2-1 Synthesis of Hexa(thiazolyl) Ligand **2***

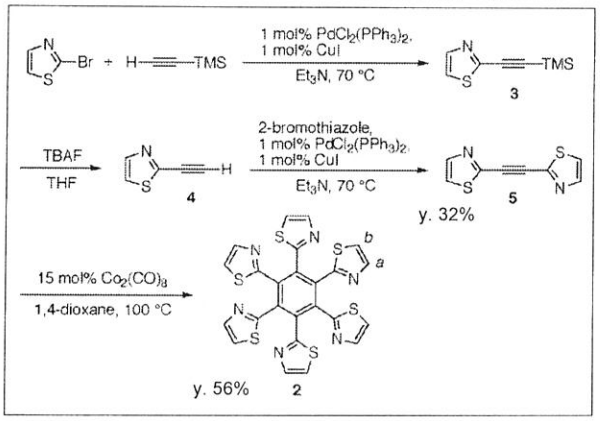

Fig. 3-2-2 ^{1}H-NMR Spectra in CD_3OD

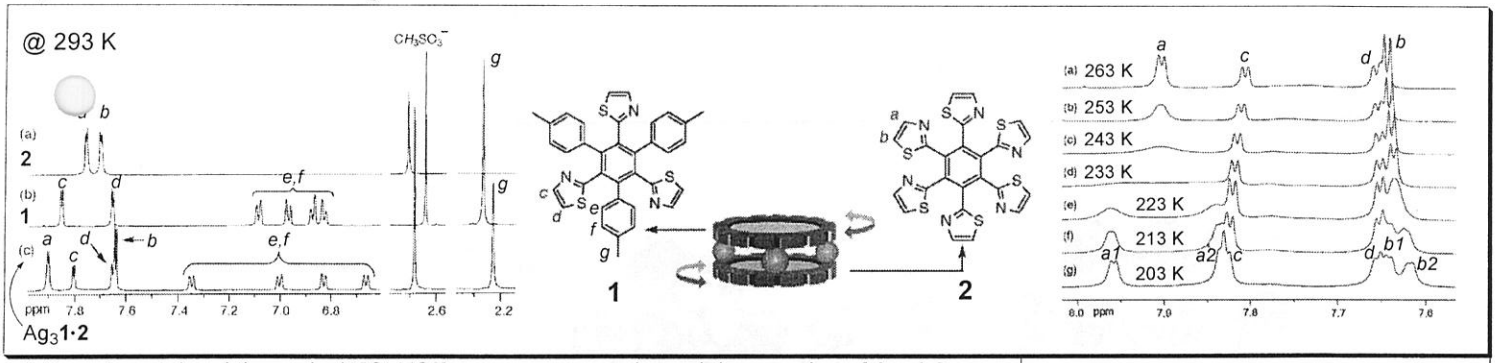

Experimental and theoretical ESI-TOF mass spectrum showed the complex of Ag_3**1**·**2**.
The complex rotates temperature-dependently.

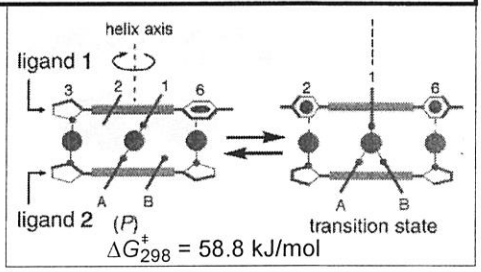

> Correlated motion of two rotor molecules

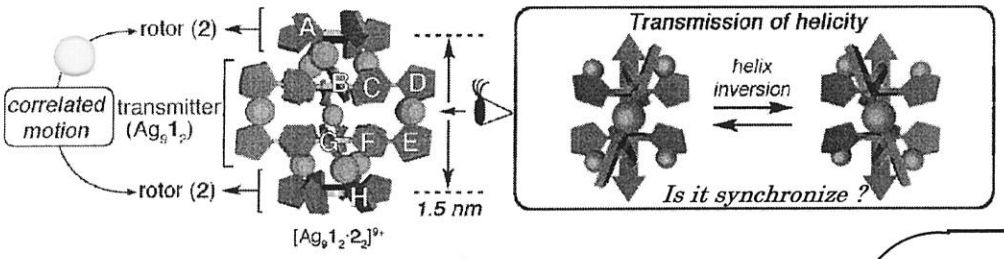

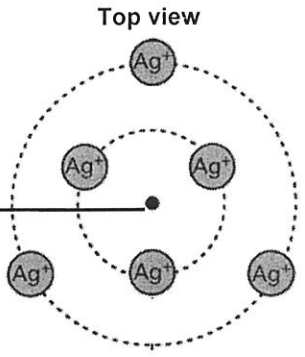

Scheme 3-2-2 Preparation of $[Ag_9\mathbf{1}_2\ \mathbf{2}_2]^{9+}$ and its Structure

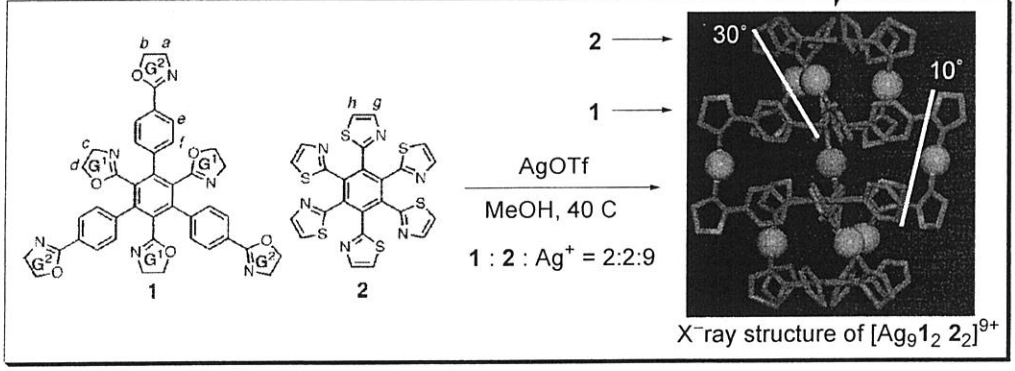

Two outer and inner disk-shaped ligands stacked on top of each other with the aid of nine Ag^+ ions.

All the ligand ring planes are not perpendicular to the centralbenzene ring planes. (They form a helical structure.)

Fig. 3-2-3 Helix Inversion

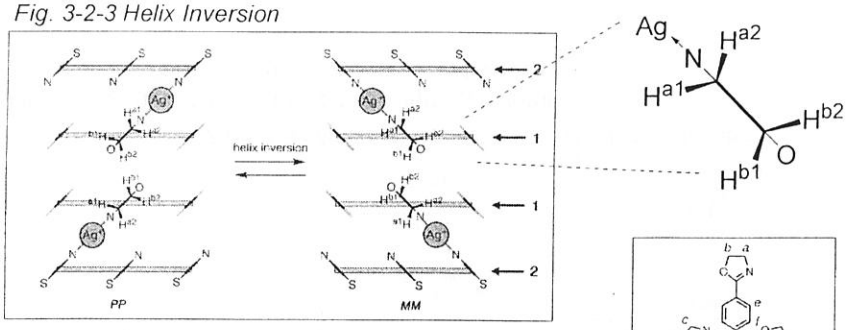

If the motion of the two terminal rotors **2** are synchronized with each other, the rates of helix inversion(k) of inner and outer rings in **1** should be identified .
This means the helix inversions of both rotor and transmitter take place at the same frequency.

Fig. 3-2-4 ^{1}H-NMR Study

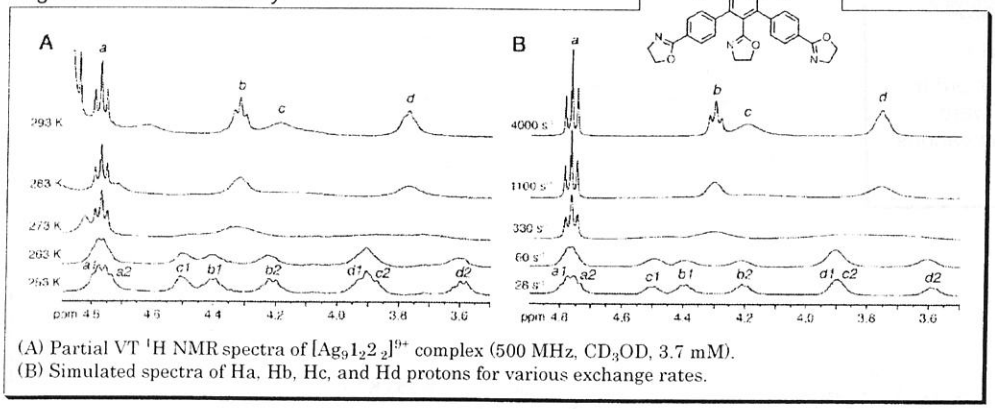

(A) Partial VT ^{1}H NMR spectra of $[Ag_9\mathbf{1}_2\mathbf{2}_2]^{9+}$ complex (500 MHz, CD_3OD, 3.7 mM).
(B) Simulated spectra of Ha, Hb, Hc, and Hd protons for various exchange rates.

As the temp of solution was lowered, the oxazolinyl proton signals, *a*-*d*, were divided into two sets.
The simulated proton signals clarify that the helix inversion of inner and outer rings takes place at almost the same rate at temp of A.

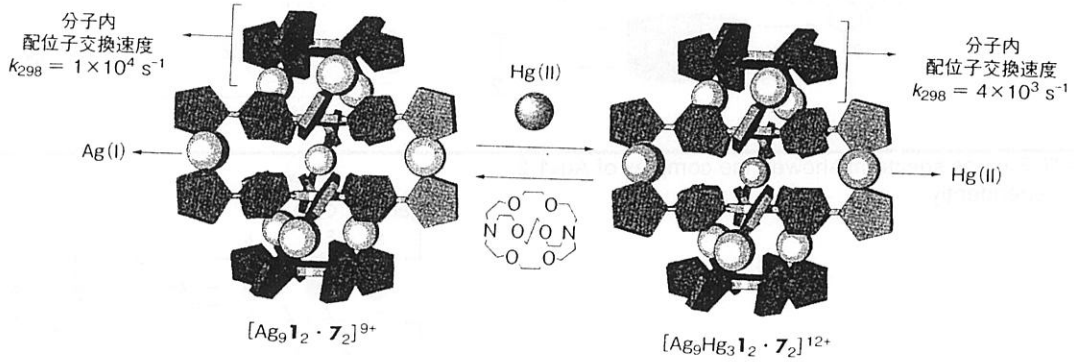

3-3. Molecular Ratchet

> Toward Unidirectional Rotation

Kelly, T. R. et al. *JACS*, **1994**, *116*, 3657
Nature, **1999**, *401*, 150 *JACS*, **2000**, *122*, 6935 etc

Fig. 3-3-1 Image of Unidirection

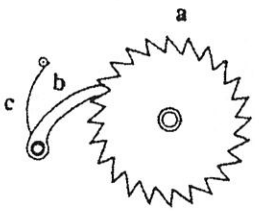

Figure 1. A simple ratchet: a) toothed wheel, b) pawl, c) spring.

Fig. 3-3-2 Chiral Gears

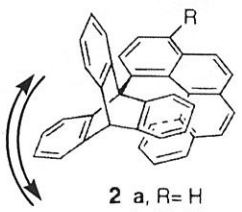

2 a, R= H
b, R= Me

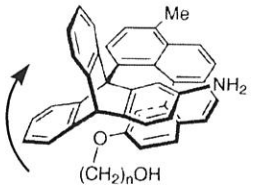

6, n = 3 (as a mixture of atropisomers)
7, n = 2 (as a mixture of atropisomers)

^{1}H-NMR peak-broadening of triptycene indicates slow rotation at 160 C.(2b)

The triptycene of **6** rotate even at the room temp.

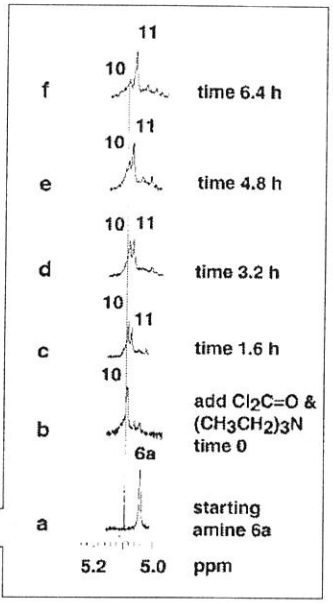

Fig. 3-3-3 Calculated Rotarional Energy

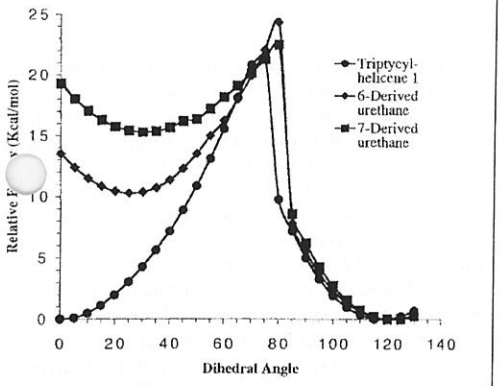

Figure 4. Calculated[26] (AM1) relative energies for rotation around the triptycene/helicene bond in **1** (●), the urethane derived from **6** (◆), and the urethane derived from **7** (■). See text for discussion.

Scheme 3-3-1

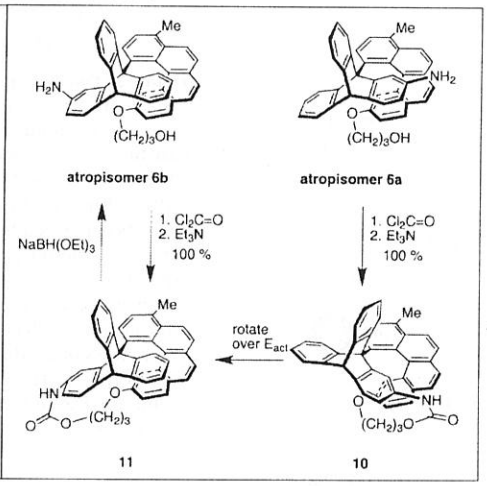

> Other Examples of Unidirectional Rotation

1) Leigh, D. A. et al. *Science*, **2004**, *306*, 1532 ⟶ Chemical and Photo-chemical Reaction.

2) Koumura, N.; Zijistra, R. W. J.; van Delden, R. A.; Feringa, B. L. et al. *Nature*, **1999**, *401*, 152
Challenge i) repetitive 360 rotation
ii) light as the source of energy
iii) unidirectionally rotation

3-3-4 Photochemical Thermal Isomerization

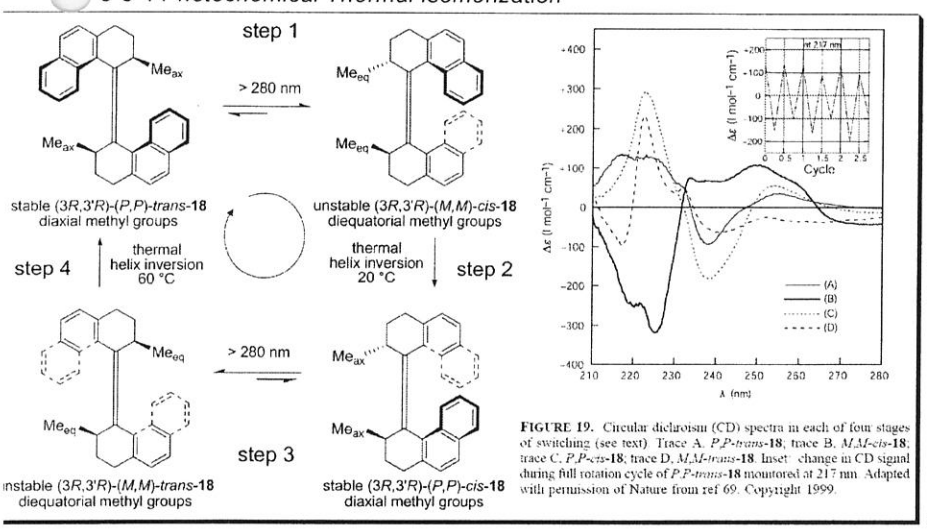

FIGURE 19. Circular dichroism (CD) spectra in each of four stages of switching (see text). Trace A, *P,P-trans*-**18**; trace B, *M,M-cis*-**18**; trace C, *P,P-cis*-**18**; trace D, *M,M-trans*-**18**. Inset: change in CD signal during full rotation cycle of *P,P-trans*-**18** monitored at 217 nm. Adapted with permission of Nature from ref 69. Copyright 1999.

Photochemical conversion of an alkene from the trans to the cis isomer is very fast. < 300 ps
It is an energetically uphill process.

The r.d.s. of cycle(Fig.3-3-4) is step 4.
$t_{1/2}$(@rt) = 78 min

⇩

The helix inversion(step4) was facilitated because of the reduced steric hindrance.

$t_{1/2}$(@rt) = 18 s

$t_{1/2}$(@rt) = 5.74 ms

This study allowed the propeller to rotate unidirectionally up to 80 rotations per second at 20 C.
(for ATPase : 160 rotations per second)

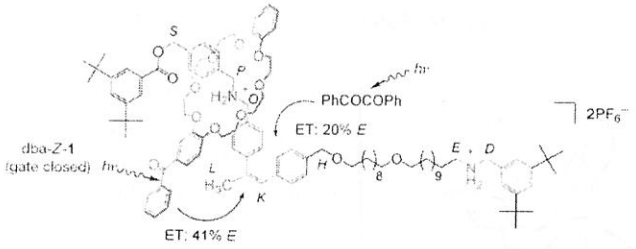

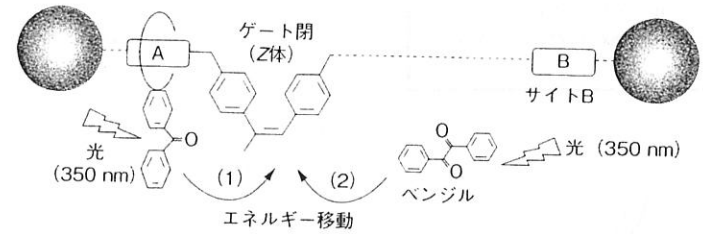

(1) 環状分子からのエネルギー移動による異性化（開：閉／＝／41：5
(2) ベンジルからのエネルギー移動による異性化（開：閉／＝／20：8

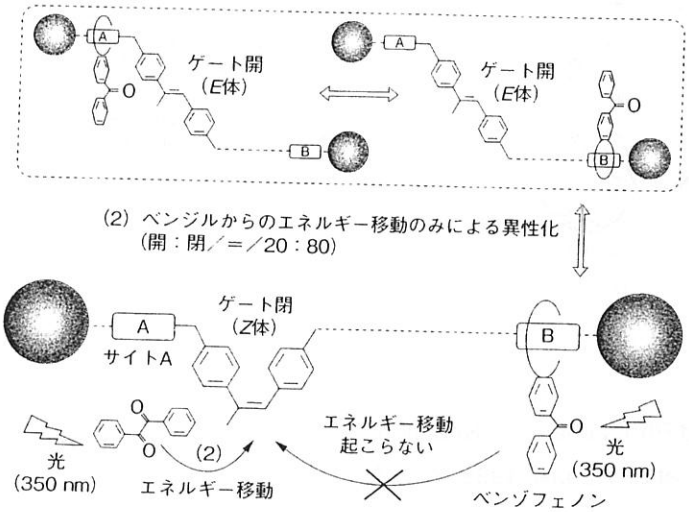

図1　情報ラチェット機構をもつ分子の駆動メカニズム

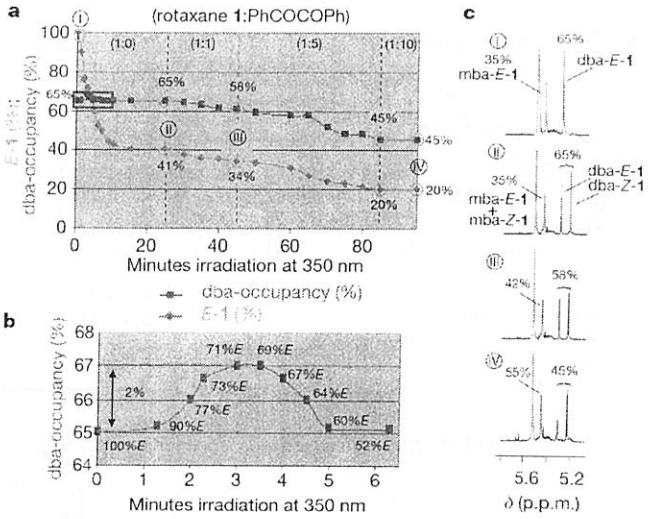

Figure 3 | Operation of a molecular information ratchet. **a**, Change in the *E*:*Z* ratio (*E*-**1** (%), the amount of the 'open gate' form of the sample, shown by purple diamonds) and the dba:mba ratio (dba-occupancy (%), shown by dark blue squares) that occurs during irradiation of **1** at 350 nm in CD_3OD, 298 K: I, pristine *E*-**1**; II, after 25 min (PSS), no added benzil; III, after a further 20 min (PSS) with 1 equiv. benzil; IV, after a further 40 min with 5 equiv. benzil plus a further 15 min (PSS) with 10 equiv. benzil. A small amount of photodegradation (≤2%) occurs over the course of the experiment, and the error in the final *E*:*Z* and dba:mba ratios is ±2%. **b**, Expansion showing the small increase (2–5%, see Supplementary Information) in dba compartment occupancy that occurs during the first five minutes of irradiation in the absence of benzil. **c**, ^{1}H NMR spectral window ($H_{s'+s}$, H_s and H_S, 600 MHz, CD_3OD, 298 K) in which the changes in both the *E*:*Z* and dba:mba ratios can be seen during the photochemistry experiment.

参照 "Molecular Switch" Ben L. Feringa
"最新分子マシン" 化学同人